Electronic supplementary Information

Elucidating the long-range charge carrier mobility in metal halide perovskite thin films

Jongchul Lim, Maximilian T. Hörantner, Nobuya Sakai, James M. Ball, Suhas Mahesh, Nakita K. Noel, Yen-Hung Lin, Jay B. Patel, David P. McMeekin, Michael B. Johnston, Bernard Wenger and Henry J. Snaith**

Clarendon Laboratory, University of Oxford, Parks Road, Oxford OX1 3PU, UK

E-mail: bernard.wenger@physics.ox.ac.uk, henry.snaith@physics.ox.ac.uk

Detail of experiments

Detail of experiments

Preparation of solution processed $CH_3NH_3PbI_3$ perovskite film: $MAPbI_3$ (termed MA-ACN) films were fabricated from the ACN/MA compound solvent following a previously published experimental protocol.[1] Briefly, MAI (Dyesol) and PbI_2 (TCI Chemicals, 99.5%) were dispersed in ACN (Sigma Aldrich 99.5%, anhydrous) in a 1:1.06 molar ratio, such that the overall concentration of the dispersion was 0.5 M. A solution of methylamine (Sigma Aldrich, 33 wt.% in ethanol) was placed into an ice bath, and using nitrogen as a carrier gas, the solution was degassed of methylamine, which was passed through a drying tube filled with desiccant (CaO and Drierite) before being bubbled into the perovskite dispersion. Methylamine gas was bubbled into the dispersion until all the solid, black crystals were dissolved, leaving a clear, yellow solution. The vial was sealed with a septum cap and the solution kept in the refrigerator at 5 ℃ until use. This film is stable in air without encapsulation for the duration of the experiment. The film average thickness is 400nm.

Preparation of $Cs_{0.17}FA_{0.83}Pb(I_{0.9}Br_{0.1})_3$ and $Cs_{0.05}(FA_{0.83}MA_{0.17})_{0.95}Pb(I_{0.9}Br_{0.1})_3$ perovskite films[2–4]: To form the mixed-cation lead mixed anion perovskite precursor solutions, caesium iodide (CsI, Alfa Aesar), formamidinium iodide (FAI, GreatCell Solar), methylammonium iodide (MAI, GreatCell Solar), lead iodide (PbI_2, TCI) and lead bromide ($PbBr_2$, Alfa Aesar) were prepared in the way corresponding to the exact stoichiometry for the desired $Cs_{0.05}(FA_{0.83}MA_{0.17})_{0.95}Pb(I_{0.9}Br_{0.1})_3$ (termed FAMACs) and $Cs_{0.17}FA_{0.83}Pb(I_{0.9}Br_{0.1})_3$ (termed FACs) compositions in a mixed organic solvent of anhydrous N,N-dimethylformamide (DMF, Sigma-Aldrich) and dimethyl sulfoxide (DMSO, Sigma-Aldrich) at the ratio of DMF : DMSO = 4 : 1. The perovskite precursor concentration used was 1.30 M. The deposition of perovskite layers was carried out using a spin coater in a nitrogen-filled glove box with the following processing parameters: starting at 1000 rpm (ramping time of 4 sec) for 10 sec and then 6000 rpm (ramping time of 6 sec from 1000 rpm) for 35 sec. 10 sec before the

end of the spinning process, a solvent-quenching method was used by dropping 300 µL toluene onto the perovskite wet films. The film average thicknesses are 495 and 550nm for FACs and FAMACs, respectively.

Preparation of co-evaporated $CH_3NH_3PbI_3$ perovskite film: $CH_3NH_3PbI_3$ thin films were deposited on glass substrates using the dual-source thermal evaporation technique as shown previously by Patel *et al*.[5,6] Briefly CH_3NH_3I and PbI_2 were placed in separate crucibles and heated under vacuum (5 x 10^{-6} mbar) until the combined vapour deposition rate was 0.4 Å/s, as measured by the quartz crystal microbalance. Once the rate stabilised, the substrates were exposed to the vapour until the desired thickness of $CH_3NH_3PbI_3$ was attained. The film average thickness is 400nm.

PITR setup and measurement: A 532 nm continuous-wave (CW) laser chopped for 70Hz by internally referenced lock-in amplifier was attenuated by OD filter for various intensity as mentioned in main text. Halogen lamp continuously irradiated on certain masked area of perovskite film for probing the periodic changes of transmission and reflection in photon energy range from 1.20 to 1.85 eV by using long pass and near-infrared (NIR) OD filters. The two identical pre-amplified photodetectors (PDA36a, Thorlabs) are installed on monochromators (Acton SP2300i, Princeton Instruments) for both transmitted and reflected photon detection. Illumination mask is placed on top of sample for focusing pulse laser pump and continuous-wave Halogen lamp probe sources on the same position. The impact of the incidence angle of irradiation for reflections at each interface is fully accounted for in the Transfer Matrix Model. Internal referenced lock-in amplifier synchronizes the measurement of transmission and reflection, for all PL and PIA, then followed by PL subtraction.

Calculation of Δn and Δk from Reflectance and Transmittance measurements: We measured the Reflectance R' and Transmittance T' for a photo excited perovskite film. This data was used to calculate the change in refractive index $\Delta n(\lambda) + i\Delta k(\lambda)$ during photo-excitation. The approach is outlined below: Let the initial complex refractive index of perovskite be $n_0(\lambda) + ik_0(\lambda)$. Upon photo-excitation, the refractive index changes to $n_1(\lambda) + ik_1(\lambda)$. To find $n_1(\lambda) + ik_1(\lambda)$, we searched through the space of possible solutions until we found the $n'(\lambda) + ik'(\lambda)$ that, when fed into an optical transfer matrix model, best reproduces the measured R_1 and T_1. This optimization was done through Powell's Algorithm with a Pythagorean distance function. The trial solutions were always chosen to be Kramers-Kronig consistent, using a numerical implementation of Maclaurin's formula for the Kramers-Kronig transform.[7] The obtained $n'(\lambda) + ik'(\lambda)$ is equal to $n_1(\lambda) + ik_1(\lambda)$, within the bounds of fitting error. It is then straightforward to calculate $\Delta n(\lambda) + i\Delta k(\lambda) = n_1(\lambda) + ik_1(\lambda) - n_0(\lambda) - ik_0(\lambda)$. We take the initial complex refractive index $n_0(\lambda) + ik_0(\lambda)$ from measurements in the literature.[8]

Quasi-steady-state photo-conductivity: A continuous diode laser was used at the range of excitation density specified in the main text, with an excitation wavelength of 532 nm and a modulation frequency of 70 Hz. A bias of 25 V was applied across the in-plane electrodes, while the current was monitored by an oscilloscope, as described in detail elsewhere.[9,10] The resistance through the oscilloscope was set by a variable resistor to always be <1% of the sample resistance. We monitored the voltage between the 2 in-plane electrodes through the variable resistor in the circuit to determine the potential dropped across channel length. We then confirmed this by photo-doing effect and frequency effect of the samples at various light intensities, as shown in the Electronic Supplementary Information (**Fig S2**). In both PITR and

the photo-conductivity measurement, the square pulse of the laser is generated by a 70 Hz chopper, resulting in a 7 ms periodic laser pulse width, which is much longer than the recombination time of charge carriers.

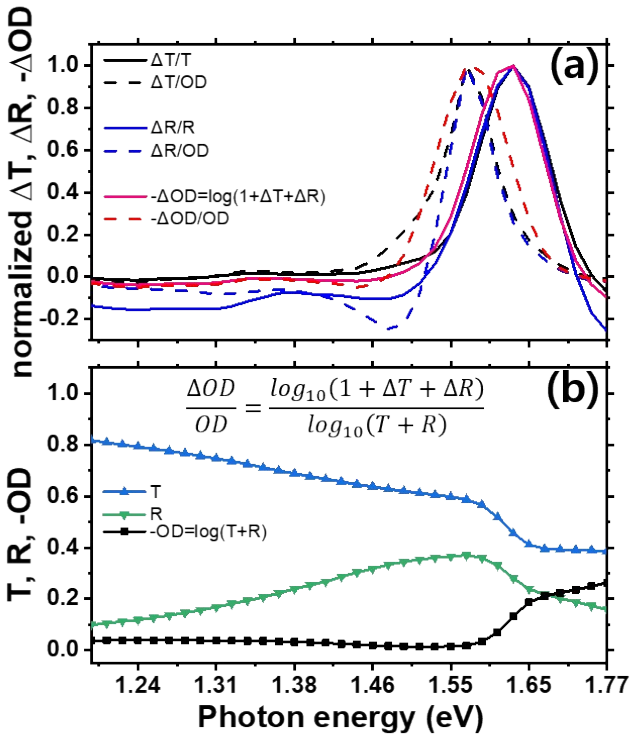

Figure S1. Shifted peak of ΔOD/OD spectrum due to shape of the OD spectrum (MA-ACN perovskite film). (a) normalized ΔT/T, ΔR/R and ΔOD spectra, and the normalized spectra of ΔT, ΔR and ΔOD divided by OD for illustrative purposes only. (b) T, R and OD spectra for the calculation of photo-induced changes

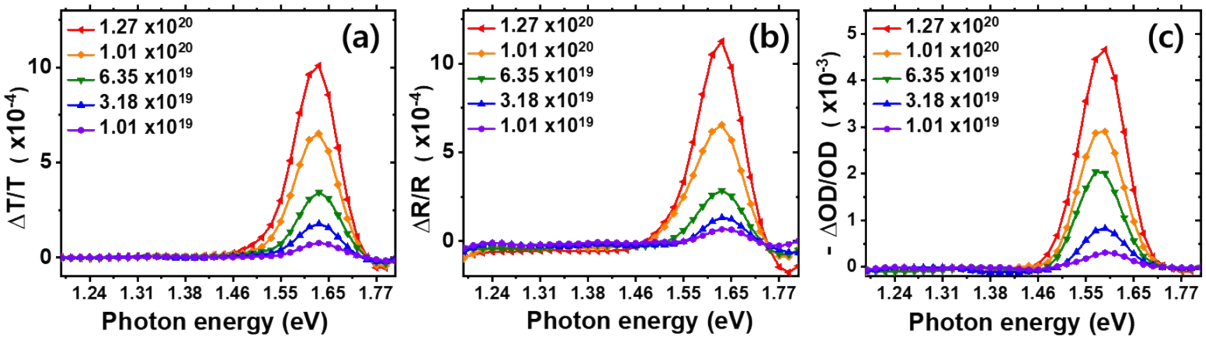

Figure S2. Photo-induced transmission and reflection changes, and corresponding optical density changes with various excitation densities for MA-ACN perovskite film. We obtained refractive index changes as a function of excitation density (photons $cm^{-3}s^{-1}$) by fitting experimental data ((a) ΔT/T, (b) ΔR/R and (c) ΔOD/OD), as described in experimental section.

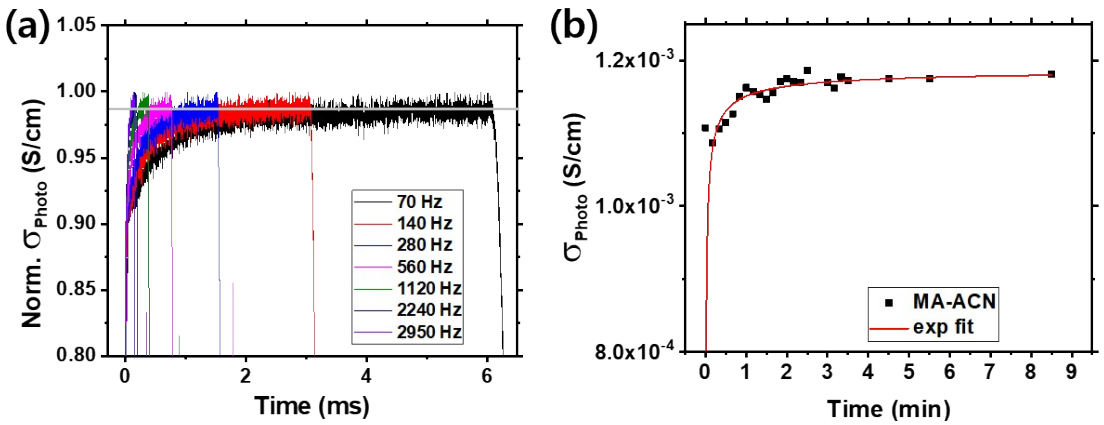

Figure S3. Photo-conductivities of MA-ACN perovskite film. (a) Chopping frequency dependent σ_{Photo}, showing that 70Hz reaches equilibrated state between generation and recombination of charge carrier as a σ_{Photo}, this indicates that the short pulse illumination time by high chopping frequency is not enough to reach the equilibrium between generation and recombination of charge carriers. (b) Time dependent increase in σ_{Photo} as a photo-doping effect.

Table S1. Photo-induced optoelectronic parameters obtained from the evaluation process as described in main text. Carrier generation rate (G) ($cm^{-3}s^{-1}$), charge carrier density (cm^{-3}), quasi-steady-state σ_{Photo} (S/cm), mobility (cm^2/Vs), pseudo-first order recombination rate (k) (s^{-1}), charge carrier diffusion length (μm), recombination time (μs). MA-ACN: $MAPbI_3$, MA-evap: $MAPbI_3$, FACs: $Cs_{0.17}FA_{0.83}Pb(I_{0.9}Br_{0.1})_3$ FAMACs: $Cs_{0.05}(FA_{0.83}MA_{0.17})_{0.95}Pb(I_{0.9}Br_{0.1})_3$.

	G ($cm^{-3}s^{-1}$)	Carrier Density (cm^{-3})	σ_{Photo} (S/cm)	Mobility (cm^2/Vs)	k (s^{-1})	Diffusion length (μm)	Recombination time (s)
MA-ACN	1.8×10^{22}	2.8×10^{16}	2.1×10^{-3}	0.47	6.4×10^{5}	1.37	1.6×10^{-6}
	1.4×10^{22}	1.6×10^{16}	1.9×10^{-3}	0.72	8.7×10^{5}	1.45	1.2×10^{-6}
	8.9×10^{21}	9.3×10^{15}	1.5×10^{-3}	1.02	9.5×10^{5}	1.66	1.1×10^{-6}
	4.5×10^{21}	4.7×10^{15}	1.2×10^{-3}	1.54	9.6×10^{5}	2.03	1.0×10^{-6}
	1.4×10^{21}	1.9×10^{15}	6.6×10^{-4}	2.19	7.5×10^{5}	2.74	1.3×10^{-6}
MA-evap	4.0×10^{22}	1.4×10^{15}	1.1×10^{-4}	0.51	2.9×10^{7}	0.21	3.4×10^{-8}
	2.8×10^{22}	8.0×10^{14}	7.8×10^{-5}	0.61	3.5×10^{7}	0.21	2.8×10^{-8}
	1.8×10^{22}	5.2×10^{14}	6.3×10^{-5}	0.76	3.4×10^{7}	0.24	2.9×10^{-8}
	8.9×10^{21}	2.7×10^{14}	5.1×10^{-5}	1.19	3.4×10^{7}	0.30	3.0×10^{-8}
FACs	2.3×10^{22}	3.1×10^{16}	1.4×10^{-3}	0.28	7.4×10^{5}	0.99	1.4×10^{-6}
	1.5×10^{22}	2.0×10^{16}	1.0×10^{-3}	0.32	7.3×10^{5}	1.06	1.4×10^{-6}
	7.3×10^{21}	1.3×10^{16}	6.3×10^{-4}	0.31	5.8×10^{5}	1.18	1.7×10^{-6}
	5.8×10^{21}	4.3×10^{15}	2.6×10^{-4}	0.38	1.3×10^{6}	0.86	7.5×10^{-7}
FAMACs	2.0×10^{22}	1.3×10^{16}	3.8×10^{-4}	0.19	1.6×10^{6}	0.55	6.2×10^{-7}
	1.3×10^{22}	9.1×10^{15}	3.3×10^{-4}	0.23	1.4×10^{6}	0.65	7.1×10^{-7}
	6.4×10^{21}	6.0×10^{15}	2.7×10^{-4}	0.28	1.1×10^{6}	0.82	9.4×10^{-7}
	5.1×10^{21}	3.5×10^{15}	1.5×10^{-4}	0.27	1.4×10^{6}	0.69	7.0×10^{-7}

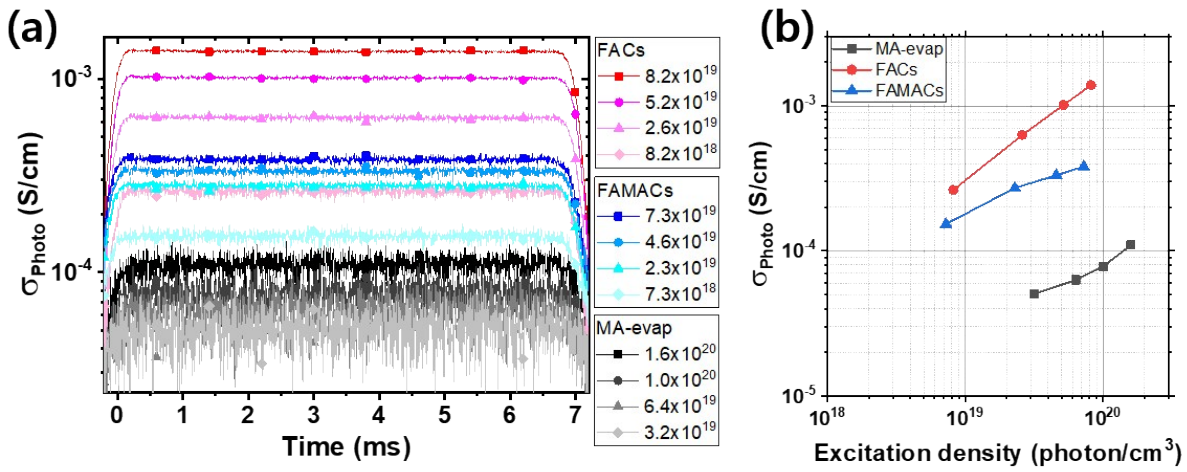

Figure S4. Photo-conductivity of three perovskite films prepared in different ways as a function of excitation density. (a) Photo-conductivity under the 7ms light illumination (70Hz modulation, excitation density: photons $cm^{-3}s^{-1}$) and (b) the corresponding photo-conductivity values as a function of excitation density (photons $cm^{-3}s^{-1}$). MA-evap ($MAPbI_3$ evaporation processed), FACs ($Cs_{0.17}FA_{0.83}Pb(I_{0.9}Br_{0.1})_3$ solution processed) and FAMACs ($Cs_{0.05}(FA_{0.83}MA_{0.17})_{0.95}Pb(I_{0.9}Br_{0.1})_3$ solution processed).

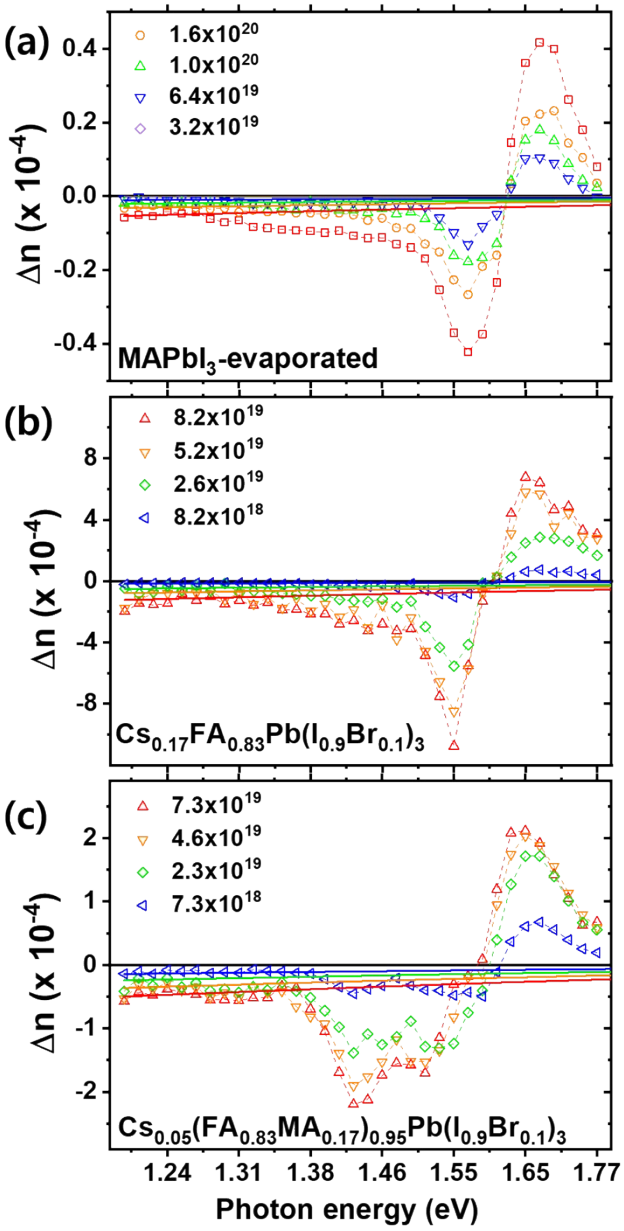

Figure S5. Excitation density (photons $cm^{-3}s^{-1}$) dependent light induced refractive index changes from experimental data (open symbol, dashed line is only to guide the eyes) and fitted data (solid lines) by optical modeling for three perovskite films; (a) MA-evap ($MAPbI_3$ evaporation processed) (b) FACs ($Cs_{0.17}FA_{0.83}Pb(I_{0.9}Br_{0.1})_3$ solution processed), FAMACs ($Cs_{0.05}(FA_{0.83}MA_{0.17})_{0.95}Pb(I_{0.9}Br_{0.1})_3$ solution processed).

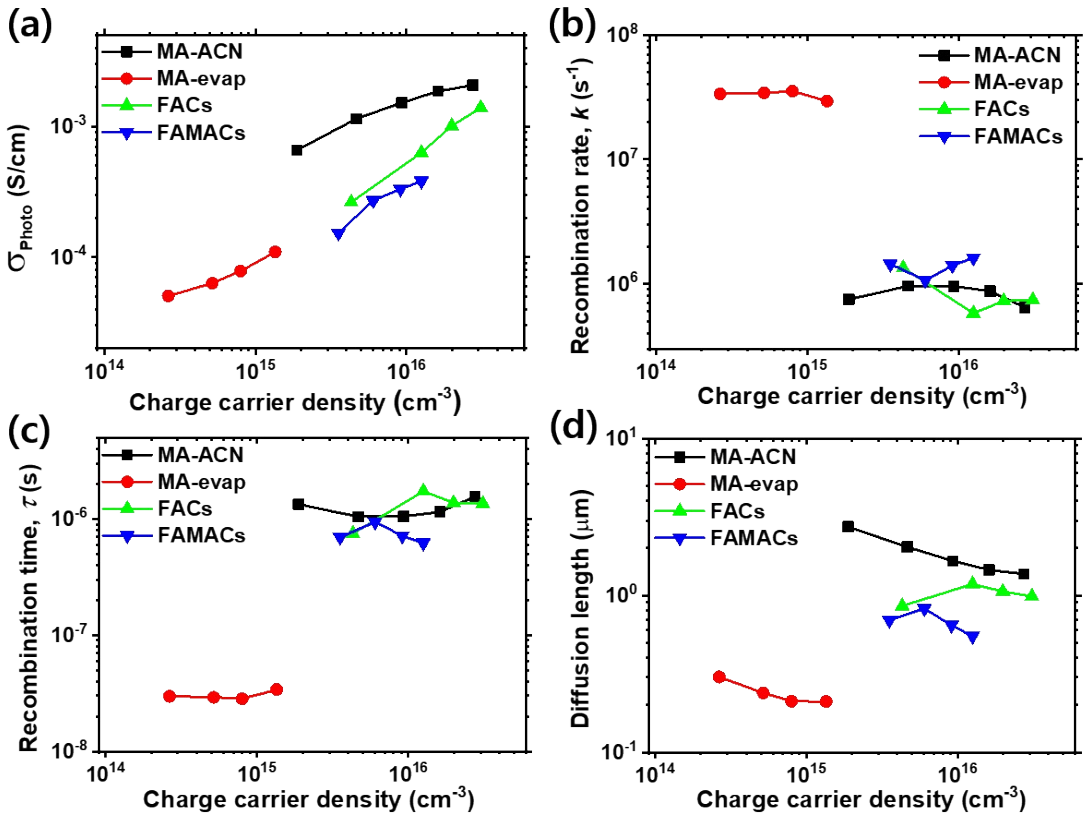

Figure S6. Photo-induced optoelectronic parameters obtained by the evaluation processes for all perovskite films in our study. (a) Photo-conductivity (S/cm), (b) pseudo-first order recombination rate (s^{-1}), (c) recombination time (s) and (d) charge carrier diffusion length (μm) as a function of charge carrier density (cm^{-3}) for MA-ACN ($MAPbI_3$-ACN solution processed), MA-evap ($MAPbI_3$ evaporation processed), FACs ($Cs_{0.17}FA_{0.83}Pb(I_{0.9}Br_{0.1})_3$ solution processed) and FAMACs ($Cs_{0.05}(FA_{0.83}MA_{0.17})_{0.95}Pb(I_{0.9}Br_{0.1})_3$ solution processed) films.

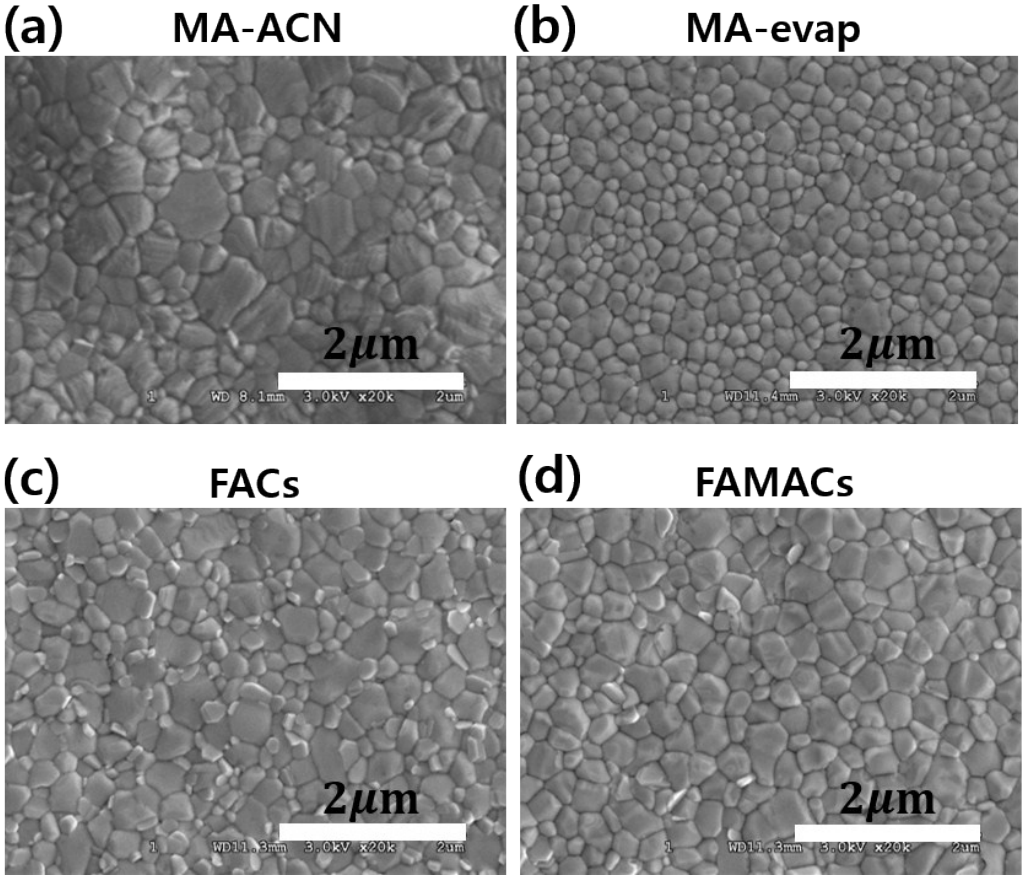

Figure S7. Top view images of perovskite polycrystalline films measured by SEM. Sizes of individual domains ranging (a) between 500 nm and 700 nm for MA-ACN film ($MAPbI_3$-ACN solution processed), (b) between 162 nm and 360 nm for MA-evap film ($MAPbI_3$-evaporated), (c) between 236 nm and 585 nm for FACs film ($Cs_{0.17}FA_{0.83}Pb(I_{0.9}Br_{0.1})_3$ solution processed) and (d) between 183 nm and 442 nm for FAMACs film ($Cs_{0.05}(FA_{0.83}MA_{0.17})_{0.95}Pb(I_{0.9}Br_{0.1})_3$ solution processed.

References

1 N. K. Noel, S. N. Habisreutinger, B. Wenger, M. T. Klug, M. T. Hörantner, M. B. Johnston, R. J. Nicholas, D. T. Moore and H. J. Snaith, *Energy Environ. Sci.*, 2017, **10**, 145–152.

2 D. P. McMeekin, G. Sadoughi, W. Rehman, G. E. Eperon, M. Saliba, M. T. Hörantner, A. Haghighirad, N. Sakai, L. Korte, B. Rech, M. B. Johnston, L. M. Herz and H. J. Snaith, *Science*, 2016, **351**, 151–155.

3 Z. Wang, Q. Lin, B. Wenger, M. G. Christoforo, Y. H. Lin, M. T. Klug, M. B. Johnston, L. M. Herz and H. J. Snaith, *Nat. Energy*, 2018, **3**, 855–861.

4 M. Saliba, T. Matsui, J. Y. Seo, K. Domanski, J. P. Correa-Baena, M. K. Nazeeruddin, S. M. Zakeeruddin, W. Tress, A. Abate, A. Hagfeldt and M. Grätzel, *Energy Environ. Sci.*, 2016, **9**, 1989–1997.

5 J. B. Patel, J. Wong-Leung, S. Van Reenen, N. Sakai, J. T. W. Wang, E. S. Parrott, M. Liu, H. J. Snaith, L. M. Herz and M. B. Johnston, *Adv. Electron. Mater.*, 2017, **3**, 1–6.

6 J. B. Patel, Q. Lin, O. Zadvorna, C. L. Davies, L. M. Herz and M. B. Johnston, *J. Phys. Chem. Lett.*, 2018, **9**, 263–268.

7 K. Ohta and H. Ishida, *Appl. Spectrosc.*, 1988, **42**, 952–957.

8 Q. Lin, A. Armin, R. C. R. Nagiri, P. L. Burn and P. Meredith, *Nat. Photonics*, 2015, **9**, 106–112.

9 T. Leijtens, J. Lim, J. Teuscher, T. Park and H. J. Snaith, *Adv. Mater.*, 2013, **25**, 3227–3233.

10 A. Petrozza, C. Groves and H. J. Snaith, *J. Am. Chem. Soc.*, 2008, **130**, 12912–12920.